The influence of quench sensitivity on residual stresses in the aluminium alloys 7010 and 7075

Jeremy Robinson, DAVID TANNER, C.E. Truman, A.M Paradowska, R.C. Wimpory

Publication date

01-01-2012

Published in

Materials Characterization;65, pp. 73-85

Title

The influence of quench sensitivity on residual stresses in the aluminium alloys 7010 and 7075

Authors

J.S. Robinson[1], D.A. Tanner[1], C.E. Truman[2], A.M. Paradowska[3], R.C. Wimpory[4]
[1] Materials and Surface Science Institute, University of Limerick, Ireland.
[2] Department of Mechanical Engineering, University of Bristol, UK.
[3] ISIS Facility, Rutherford Appleton Laboratory, Didcot, UK
[4] Helmholtz Centre Berlin for Materials and Energy, Hahn Meitner Platz 1, Berlin, Germany
Corresponding author
J.S. Robinson
Materials Surface Science Institute,
University of Limerick,
Ireland.
Email; jeremy.robinson@ul.ie
Telephone; +353 61 202240
Fax; +353 61 338172

Keywords

Residual stress, neutron diffraction, incremental deep hole drilling (iDHD), 7010, 7075, aluminium alloys, quench sensitivity.

Abstract

The most critical stage in the heat treatment of high strength aluminium alloys is the rapid cooling necessary to form a supersaturated solid solution. A disadvantage of quenching is that the thermal gradients can be sufficient to cause inhomogeneous plastic deformation which in turn leads to the development of large residual stresses. Two 215 mm thick rectilinear forgings have been made from 7000 series alloys with widely different quench sensitivity to determine if solute loss in the form of precipitation during quenching can significantly affect residual stress magnitudes. The forgings were heat treated and immersion quenched using cold water to produce large magnitude residual stresses. The through thickness residual stresses were measured by neutron diffraction and incremental deep hole drilling. The distribution of residual stresses was found to be similar for both alloys varying from highly triaxial and tensile in the interior, to a state of biaxial compression in the surface. The 7010 forging exhibited larger tensile stresses in the interior. The microstructural variation from surface to centre for both forgings was determined using optical and transmission electron microscopy. These observations were used to confirm the origin of the hardness variation measured through the forging thickness. When the microstructural changes were accounted for in the through thickness lattice parameter, the residual stresses in the two forgings were found to be very similar. Solute loss in the 7075 forging appeared to have no significant effect on the residual stress magnitudes when compared to 7010.

Introduction

One of the unavoidable end results arising from the heat treatment of precipitation hardened aluminium alloys is the introduced of high magnitude residual stresses. Severe thermal gradients arise when thick section products are rapidly quenched from the solution heat treatment temperature. These gradients cause inhomogeneous plastic flow to occur, which in turn produces distortion and residual stresses.[1, 2] For a rectilinear block like those investigated here, immediately after quenching tensile plastic strains occur initially at the rapidly cooling edges of the material. The plastic zone then expands to cover all the rapidly cooling surfaces. The block at this point consists of a soft hot interior surrounded by a harder and cooler exterior stretched shell. As the central region starts to cool, it tries to contract but is constrained by the hard outer shell and also undergoes tensile plastic deformation. As the block cools further, the magnitude of surface plastic strains diminish as a compressive stress is developed, finally resulting in a surface stressed into compression and a centre into tension.[3] The final stress pattern is a reflection of the geometry of the component and of the temperature gradients generated throughout in the quench.

When applied to heat treatable aluminium alloys, the term quench sensitivity is a relative measure of the loss of solute from solid solution as precipitation, occurring during quenching from the solution heat treatment temperature.[4] The alloy 7075 (registered in 1954) is classed as being quench sensitive while 7010 (registered in 1975) is far less so. This is illustrated in the time-temperature property curves presented in Figure 1.[5] These “C curves” show the times required to precipitate sufficient solute to change the strength by a specified amount, in this case to give strengths of 70% and 99.5% of that achievable in material quenched infinitely quickly. Precipitation that occurs during quenching changes the subsequent response of the material to aging, but can also potentially influence the magnitude of the residual stress distribution introduced by rapid cooling by lowering the flow stress.[6] This investigation examines the residual stress distribution and magnitudes in two large rectilinear 7010 and 7075 forgings. The forgings were cold water quenched (CWQ) to induce a large residual stress which was then characterised using neutron diffraction at the ENGIN-X instrument located at ISIS, UK. The residual stresses were then also determined using the incremental deep hole drilling method (iDHD) at the University of Bristol, UK. The cores extracted during iDHD were then analysed for lattice parameter variations using neutron diffraction on the E3 instrument at the Helmholtz Centre in Berlin.

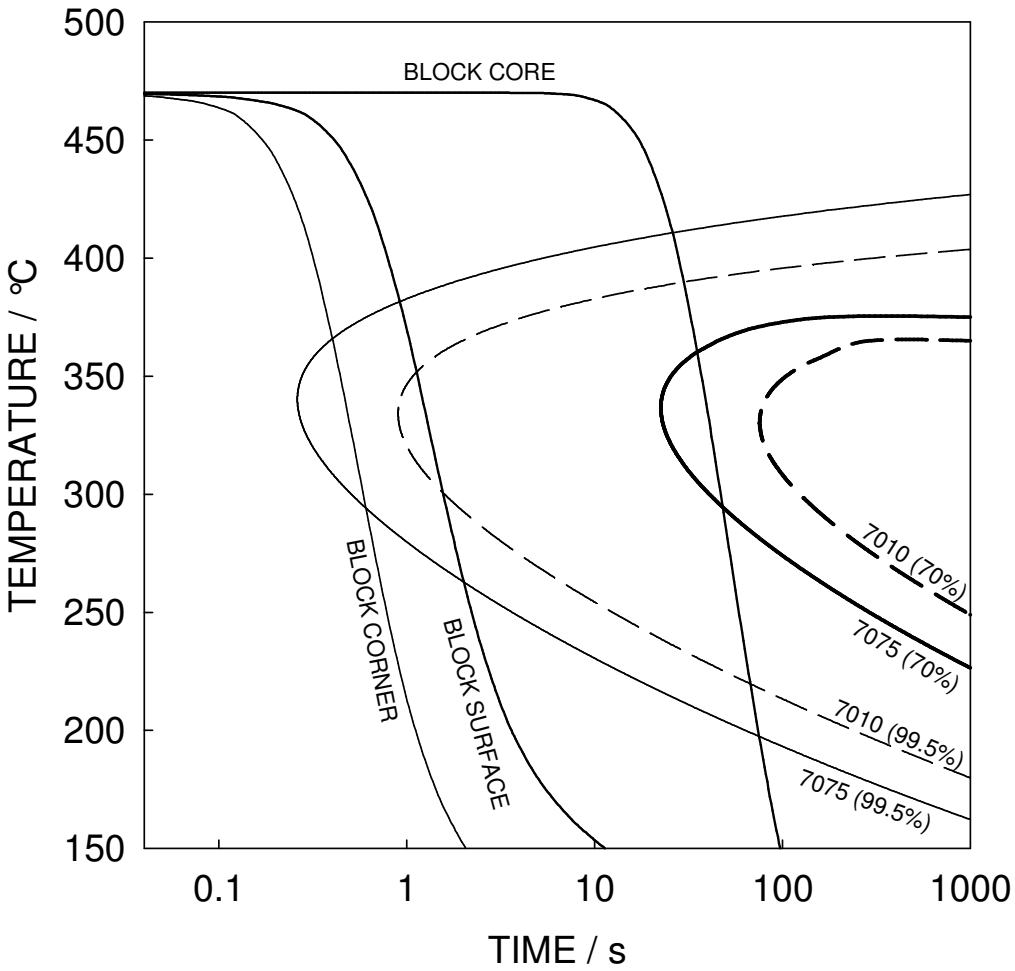

Figure 1 Time-temperature property curves for overaged 7010 and 7075. Each alloy has two TTP curves in this figure, the 99.5% curves are the locus of times required to produce 99.5% of the tensile properties associated with an infinitely fast quench. The other curves are for the times to produce 70% of the tensile properties produced by an infinitely fast quench. The cooling curves correspond to the core and corner of the rectilinear forgings investigated here, and the centre of a 300 x 215 mm surface.

2 Experimental procedures

2.1 Material details

Two rectilinear forged blocks were studied. Each forging was approximately 215 x 215 mm and 300 mm long as shown in Figure 2. The specification alloy chemistry of 7010 and 7075 is shown in Table 1.

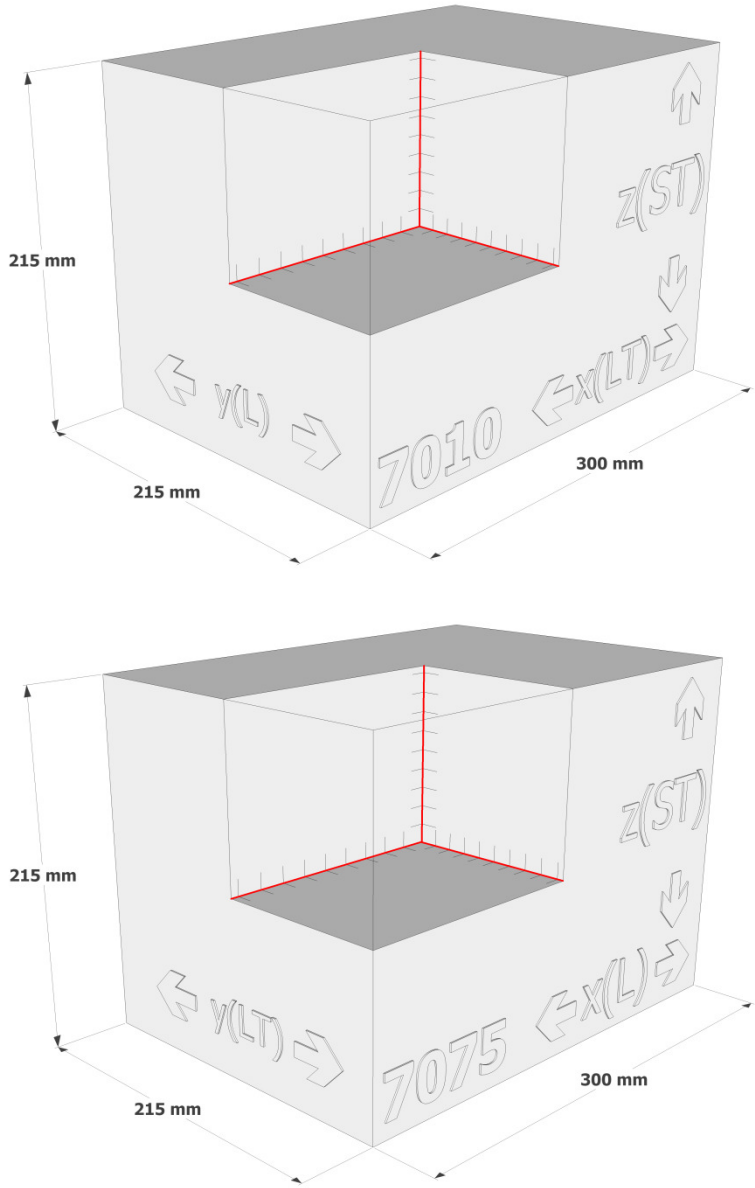

Figure 2. Dimensions of forgings and the directions along which residual strain measurements were made, originating at the central vertex.

Both samples had been manufactured from cast slab and triaxially forged. The 7010 block was sectioned from a much larger rectilinear forging whereas the 7075 block was forged from slab as a separate entity. Relative to the cast slab material origin and forging procedures, for the 7010 forging *x* = LT (long transverse), *y* = L (longitudinal) and *z* = ST (short transverse). For the 7075 forging *x* = L, *y* = LT and *z* = ST. Due to the forging method, neither forging was expected to show pronounced grain elongation. Both forged blocks were solution heat treated at 470°C and immersion cold water quenched to room temperature. Quenching was accompanied with mild agitation of the water and the water temperature was < 20°C. The forgings were not artificially aged and hence naturally aged during the experiment. This condition is referred to the W temper (unstable aging). Forging and heat treatment was carried out by Mettis Aerospace Ltd, Redditch, UK. Each forging had a mass of approximately 39 kg with a surface area of 0.35m^2. The Biot number estimated for the cold water quench was approximately 2.6. The Biot number is a dimensionless number that gives an index of the ratio of the heat transfer resistances inside and at the surface of a body. If the Biot number is > 0.1 then the thermal gradients are significant within the body. The Biot number was calculated using a characteristic linear dimension for the forgings of 40 mm (ratio of block volume to surface area), an average thermal conductivity of 180 Wm^{-1}K^{-1} and an average heat transfer coefficient of 12000 Wm^{-2}K^{-1} calculated from quenching experiments.

Alloy	wt%Zn	wt%Mg	wt%Cu	wt%Zr	wt%Fe	wt%Si	wt%Ti	wt%Mn	wt%Cr
7010	6.7-5.7	2.6-2.1	2.0-1.5	0.16-0.10	0.15max	0.12max	0.06max	0.10max	0.05max
7075	6.1-5.1	2.9-2.1	2.0-1.2	0.05max	0.5max	0.4max	0.2max	0.3max	0.3-0.2

Table 1. Specification alloy chemistry of 7010 and 7075.

The microstructure of the 7010 forging consisted of approximately "pancake" shaped grains flattened in the short transverse direction with the mean grain length in this direction being 85 µm as shown in Figure 3. In the longitudinal and long transverse the grain characteristic dimension was 160 µm. Within these grains a substructure was observed consisting of well defined polygonised equiaxed sub-grains. The mean diameter of the sub-grains was <30 µm. Other coarse phases noted were fragmented Al-Cu-Fe constituent particles and a very small volume fraction of undissolved $MgZn_2$.

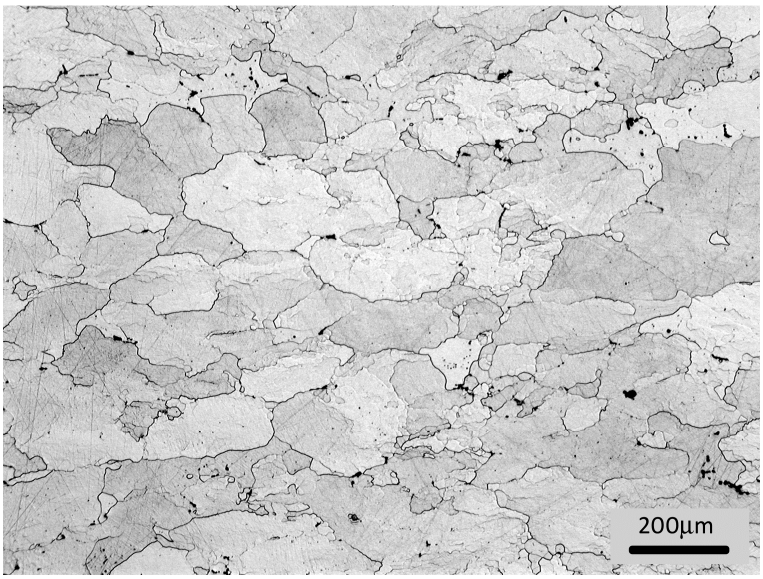

Figure 3. Microstructure of the 7010 forging. The long dimension of the picture corresponds to the longitudinal direction (y) and the short direction corresponds to the short transverse (z). Etched with Keller's reagent.

The microstructure of the 7075 forging consisted of approximately equiaxed shaped grains with the mean grain size being 86 µm as shown in Figure 4. The difference in grain size and shape between the two forgings reflects the different triaxial forging practices used. A substructure was also observed, again consisting of well defined polygonised equiaxed sub-grains. The mean diameter of the sub-grains was <20 µm, noticeably smaller than the 7010 sub-grains. Coarse phases were also observed, being present in a significantly greater volume fraction compared to 7010, a consequence of the higher combined iron and silicon content in 7075. Both microstructural samples were from the same location as the strain free reference used for neutron diffraction measurements.

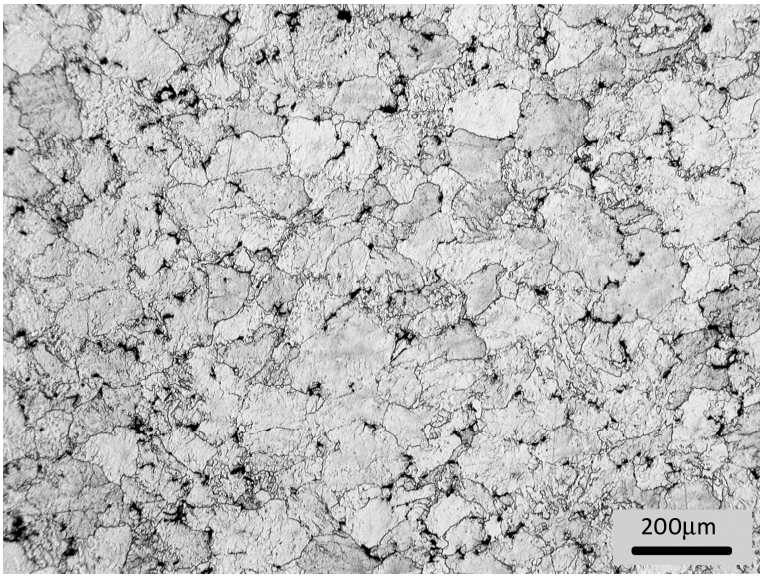

Figure 4. Microstructure of the 7075 forging. The long dimension of the picture corresponds to the longitudinal direction (x) and the short direction corresponds to the short transverse (z). Etched with Keller's reagent.

2.2 Transmission electron microscopy

Slices cut from positions in the incremental deep hole drilled cores (see section 2.5 later) corresponding to the centre and surface of the forgings were mechanically ground to a thickness of approximately 150 µm from which discs of 3 mm diameter were punched. The material was in the naturally aged (W) condition. The cooling curves associated with these locations are those shown in Figure 1. These discs were then electropolished to perforation using a Struers Tenupol-5 in a solution of 22% HNO_3 and 78% CH_3OH at −30°C. Bright-field images were taken using a JEOL 2011 transmission electron microscope operating at 200 kV.

2.3 Neutron diffraction

Measurements were made following the guidelines present in recently published guides.[7, 8] Neutron diffraction was performed on the ENGIN-X instrument at ISIS, Rutherford Appleton Laboratory, Didcot, UK, using a sampling gauge volume of 4 x 4 x 4 mm^3 as defined by the incident beam slit width and height, and the diffracted beam radial collimators. The number of grains contained in this volume was estimated at 3 x 10^4 and 1 x 10^5 for 7010 and 7075 respectively. The forgings were positioned to permit measurements of strains in the three primary working orthogonal directions of the forgings. These directions were assumed to be the principal stress directions being coincident with the direction of maximum heat flow out of the forging surfaces during quenching. The measurements originated from the vertex at the centre of the forgings, moving out to the faces with the directions following the primary mechanical working directions *x, y* and *z* as shown in Figure 2. Ten strain measurements were made along each line.

As ENGIN-X is a time-of-flight instrument, the positions of multiple diffraction peaks with coincidental scattering vectors are measured. This permitted the use of either single peak fitting or full pattern analysis through the Rietveld method with the General Structure Analysis System(GSAS),[9] which is used by the Open Genie calculation routine available on ENGIN-X. The full pattern refinement leads to the determination of an average lattice parameter, a_i based upon the position of all available peaks, where *i* is the sampled direction relative to the specimen; *i=x,y,z*. The refinement enabled the calculation of the lattice parameter using reflections from up to ten sets of interplanar spacings; (111 through to the 511). This has the potential to reduce the effects of elastic anisotropy (small for aluminium) and the influence of plastic anisotropy due to intergranular strains. Conducting a 311 single peak analysis indicated that the difference in residual stress between this analysis and the full pattern refinement was within the experimental uncertainties. This is consistent with other studies since the 311 reflection tends to exhibit low intergranular strains.

Initial d^0 measurements were performed on a small cube sample cut from the corner of each forging after heat treatment. This location would be expected to undergo the most rapid cooling during quenching. Lattice spacings were converted to residual strains and stresses using the standard three dimensional Hooke's law as shown in the equations below.[10] A Young's modulus (E) of 70 GPa and a Poisson's ratio (ν) of 0.3 was used in all the calculations.

$$\sigma_{xx} = \frac{E}{1+\nu}\varepsilon_{xx} + \frac{E\nu}{(1+\nu)(1-2\nu)}\left(\varepsilon_{xx} + \varepsilon_{yy} + \varepsilon_{zz}\right) \quad (1)$$

$$\sigma_{yy} = \frac{E}{1+\nu}\varepsilon_{yy} + \frac{E\nu}{(1+\nu)(1-2\nu)}\left(\varepsilon_{xx} + \varepsilon_{yy} + \varepsilon_{zz}\right) \quad (2)$$

$$\sigma_{zz} = \frac{E}{1+\nu}\varepsilon_{zz} + \frac{E\nu}{(1+\nu)(1-2\nu)}\left(\varepsilon_{xx} + \varepsilon_{yy} + \varepsilon_{zz}\right) \quad (3)$$

Multiple (repeatability) neutron diffraction measurements on the forgings and the associated stress free samples allowed an estimation of one standard deviation random uncertainties as ± 25 MPa.

2.4 X-ray diffraction

Surface residual stress characterisation using a local strain technique was performed on a Philips X'Pert x-ray diffractometer using Cu Kα radiation operating in the ω configuration. The measurement procedures followed were those documented in a best practice guide.[11] The position of the peak arising from diffraction from the Al 422 planes was measured (136°<2θ<139°). 14 scans were performed for each stress measurement using different ψ values within the range 0≤ψ≤50° (positive tilting only, ψ - angle between the surface normal and the bisector of source and diffracted x-ray beam). Peak locations were determined using a Pearson VII fitting technique. In all cases these fourteen peak positions were used to calculate the straight line d (lattice spacing) versus $\sin^2\psi$ plots. The calculation of residual stress from the measured peak position was made using standard theory.[12] The elastic constants were taken from literature for the 422 planes.[13] A total of 18 measurements were made on each forging, some measurements being repeated to assess the experimental uncertainties. The average of these repeated measurements is reported. The component of surface residual stress sampled was the σ_{xx} and the σ_{zz} in the centre of the face bounded by the x and z directions and the σ_{yy} and the σ_{zz} in the centre of the face bounded by the y and z directions. The x-ray measurements were completed after the deep hole measurements but were made on faces assumed to be unaffected by the gun drilling and trepanning (see section 2.5 later). The irradiated area was in the form of a line approximately 2mm thick and 12 mm long. The penetration depth of the x-rays was assumed to be of the order of 100µm calculated using reference data.[14]

2.5 Incremental deep hole drilling (iDHD)

The conventional deep hole drilling (DHD) technique is a semi-destructive mechanical strain relaxation (MSR) technique that involves drilling a hole through the thickness of the component, measuring the diameter of the hole at many angular positions and depths, trepanning a core of material from around the hole and finally re-measuring the diameter of the hole at the same angles and depths. The changes in hole diameter, caused by the relaxation of residual stress, are used to determine the residual stresses along the line of the initial hole. The DHD technique is particularly suitable for measurements in large components, being capable of determining residual stresses in specimens up to around 750 mm thickness. Full details of the conventional DHD measurement technique and several examples of its application are given in reference [15].

The conventional DHD measurement technique, as with all residual stress measurement techniques involving material removal, is based on the assumption that the corresponding change in strain occurs elastically. This

being the case, the residual stresses may be calculated directly from the measured changes in strains. However, if the residual stresses are close to yield, material removal may cause plasticity and no simple relationship exists to link the change in strain to residual stresses. A recent advance of the DHD technique, called incremental deep hole drilling (iDHD), has been developed specifically to enable measurements of residual stress in thick-sectioned components when the residual stress state is multi-axial and close to yield.[16] Full details of the iDHD technique are given in reference [17].

An incremental DHD measurement was performed on both forgings. A 3.18 mm diameter reference hole was drilled through the centre of the forgings in the *z* (ST) direction using a gun drill, as illustrated in Figure 5. The diameter of this reference hole was then accurately measured at 9 angular positions every 0.2 mm through the thickness of the forgings using an air probe. A hollow electric discharge machining tool with 10 mm diameter was then used to introduce a circular cut, or trepan, coaxially around the reference hole. Unlike a standard DHD measurement, the circular cut was introduced incrementally to a distance of 12 mm. The reference hole diameter was re-measured using the air probe at the same angular positions and depths as previously with diameter measurements being made after each increment for the iDHD measurements. In both cases, the hole diameters were then used to calculate strains and these were then transformed into σ_{xx}, σ_{yy} and τ_{xy}. It was assumed after extraction from the forgings that the deep hole drilled cores were stress free.

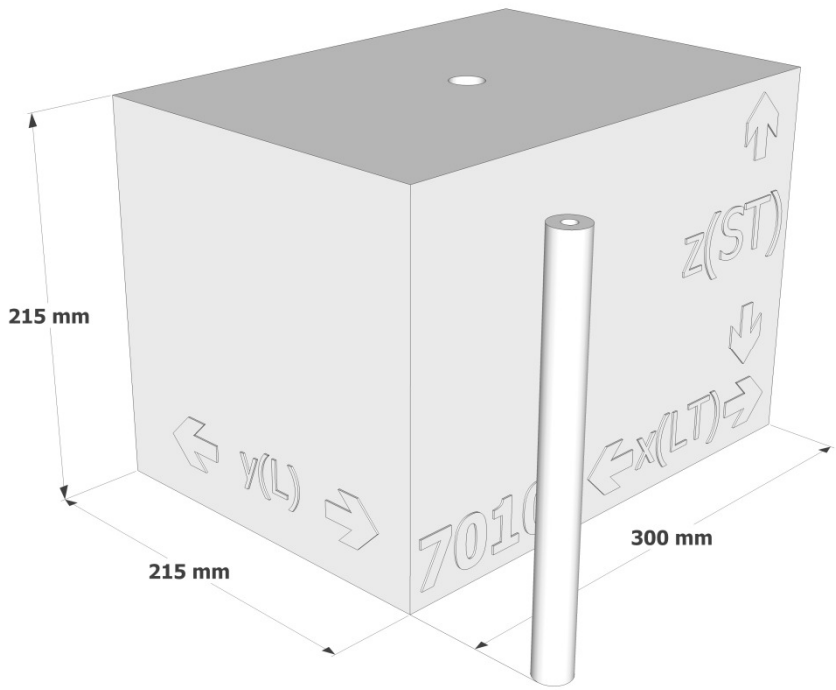

Figure 5 Location of iDHD core extracted from the forgings. The 10 mm diameter extracted core is shown in the foreground.

The hollow cores extracted during the deep hole drilling measurement were subsequently examined on the E3 instrument of the Helmholtz Centre. The lattice parameter variation along the core was measured in three orthogonal directions again corresponding to primary working directions of the original forging. The 311 aluminium matrix peak was used for all measurements. A gauge volume of approximately 3×3×3mm^3 was used in conjunction with monochromatic radiation of wavelength of 1.48Å. The gauge volume was kept as far away as possible from the electro-discharge machined surface.

2.6 Residual stress and distortion prediction using FEA

A finite element model developed using the ABAQUS[18] commercial software, was constructed to predict the residual stress distribution after cold water quenching. An isotropic rectilinear block measuring 215 x 215 x 300 mm at 470°C was chosen as the starting geometry. With the use of displacement boundary conditions,

one-eighth of the full block was modelled with 14520 eight-noded quadratic brick elements as determined through mesh density experiments (heat transfer – type DC3D8; stress displacement – type C3D8).

The analysis method employed by ABAQUS to predict residual stress distributions from quenching is uncoupled in that the temperature and displacement problems are solved consecutively. Results from the thermal analysis are read at the beginning of the stress/displacement analysis and provide the displacement loading through thermal contraction. This thermal contraction results in the development of elastic and plastic strains from which residual stresses can be calculated.

2.6.1 Heat transfer analysis

Temperature dependent properties for specific heat capacity (C_p)[19], thermal conductivity (k)[20] and density (ρ)[21] are all readily available in literature for aluminium alloys. The heat transfer coefficient (h) acts as the main boundary condition on the finite element model as it determines the rate at which heat leaves the forging surface. As this parameter varies for different quenchant temperatures and conditions, it was calculated using an inverse technique with both INTEMP[22] and ABAQUS software, resulting in the same curve in both cases. Comparison of experimental and predicted cooling curves for different rectilinear forgings of aluminium alloys has indicated that the heat transfer model accurately predicts cooling during the quench.

2.6.2 Stress-displacement analysis

Values for the thermal expansion coefficient (α_{th})[23], elastic modulus (E)[24] and Poisson's ratio (ν)[24] of 7000 series alloys were taken from literature. The elastic modulus and the thermal expansion coefficient were input as a function of temperature while Poisson's ratio was assumed to remain constant. During the quenching of aluminium alloys, the material is plastically deformed at low strain rates, the degree of which determines the final magnitude of residual stress. Unlike the elastic behaviour, the elevated temperature flow stress of 7010 and 7075 is strain rate dependent. Upper and lower bound flow stress values were calculated from the constitutive equation constants supplied by Sheppard and Jackson.[25] Data for 7050, 7150 and 7075 was used. Data for 7010 is not available but this alloys has very similar chemistry to 7050 and 7150.

At high temperatures, 7000 series alloys can be assumed to be strain rate dependent and follow a perfectly plastic stress–strain curve. As temperatures approach room temperature strain rate dependency begins to become negligible and work hardening begins to influence the stress-strain response of the material. Therefore, the input data was modified to incorporate work hardening and is assumed to be strain rate independent at room temperature. This was achieved through the use of tensile test data measured directly after quenching. Data was incorporated into the model using a lookup tabulated format.

3 Results

3.1 Residual stress characterisation

The residual stresses measured in the two forgings as a function of position within the forging are presented in Figure 6. The residual stresses are presented as three individual figures from the line scans in the *x, y* and *z* directions. For each measurement location three residual stresses are reported σ_{xx}, σ_{yy} and σ_{zz}, also corresponding to the principal directions of the forging. The distribution of the residual stresses can be described as biaxial compressive near the surface and triaxial tensile at the core. This pattern of residual stress distribution has been demonstrated by finite element modelling,[21] and confirmed by other investigators using neutron diffraction.[26] [27]

Considering the residual stresses measured during the x direction line scan, it is noted that the magnitudes of σ_{xx} in 7010 vary from +350 MPa in the centre to +30 MPa towards the surface. For 7075 the variation is +240 to -10 MPa. The σ_{xx} magnitudes tend to zero as the end face is approached as this is a free surface. The σ_{yy} and σ_{zz}, components display behaviour consistent with the symmetry of the forgings. In the 7010 forging, the

σ_{yy} and σ_{zz}, magnitudes are tensile in the core (170 and 180 MPa) and compressive in the surface (-200 and -240 MPa). For the 7075 forging, the magnitudes are 50 and 70 MPa in the core and -220 and -221 MPa at the surface. X-ray characterisation of σ_{yy} and σ_{zz} on the surface of the forgings give residual stresses consistent with the neutron diffraction measurements for both alloys. This pattern of behaviour was repeated for the *y* and *z* line scans. In summary the neutron diffraction residual stress magnitudes indicated that the core tensile residual stresses for 7010 were always larger than those for 7075. In contrast the surface compressive residual stresses were of very similar magnitude for both alloys.

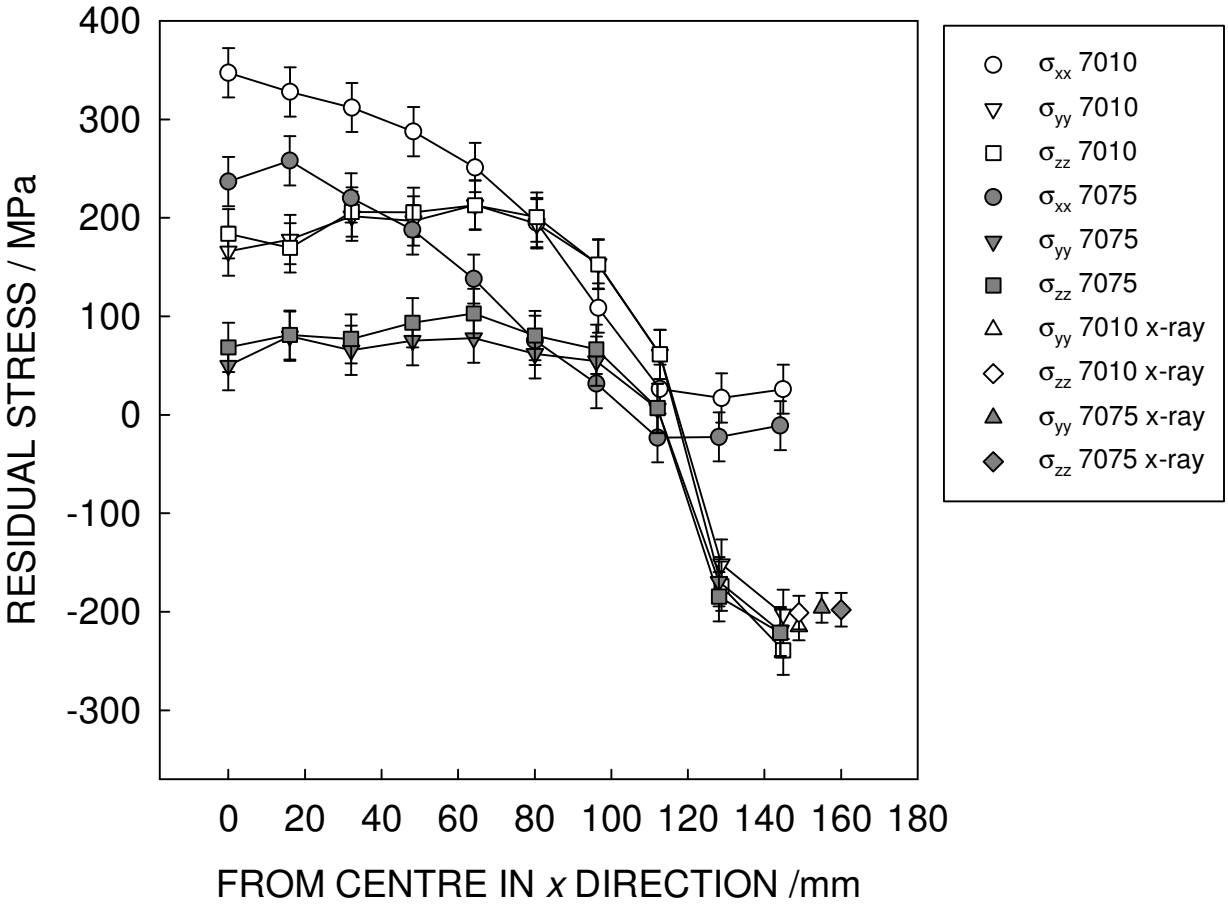

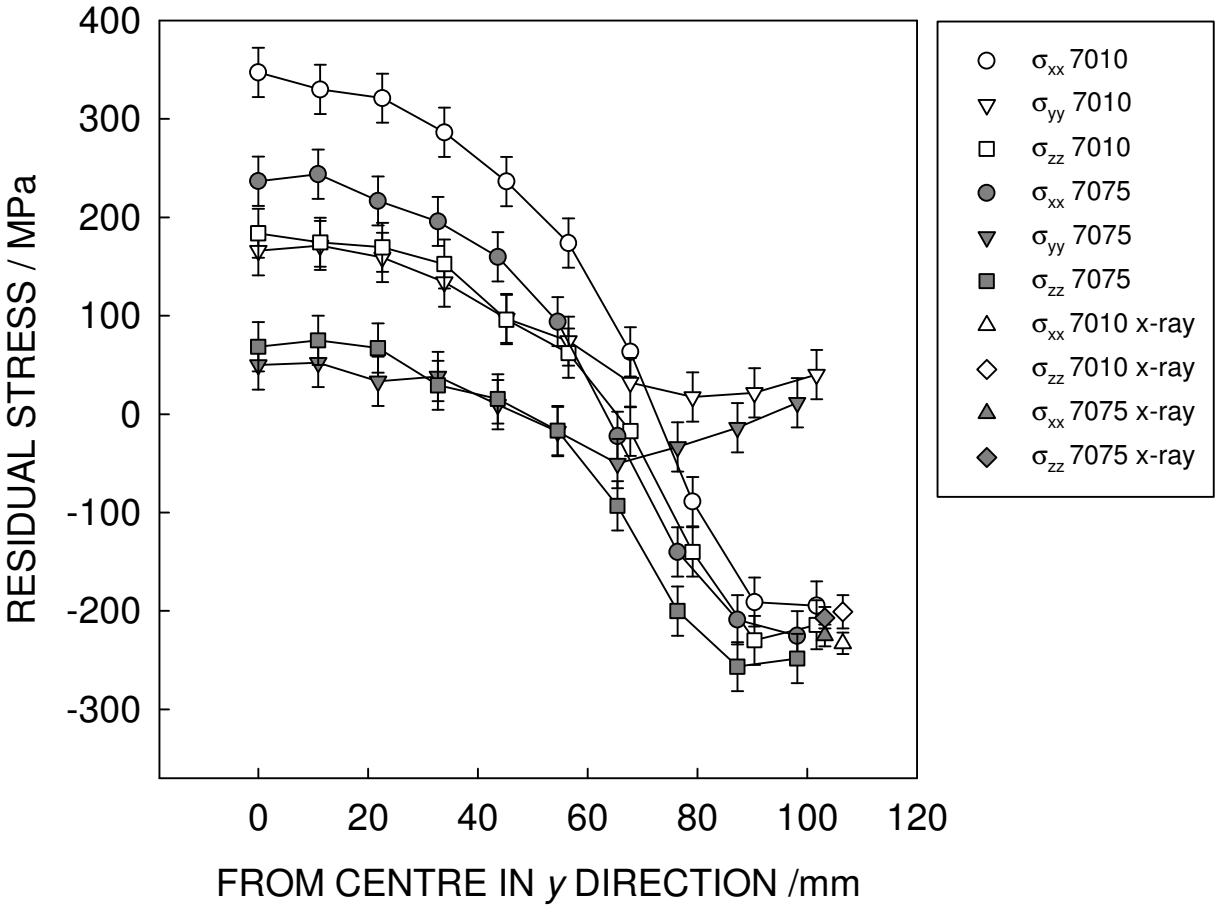
400
300
200
100
0
-100
-200
-300
RESIDUAL STRESS / MPa
0
20
40
60
80
100
120
FROM CENTRE IN y DIRECTION /mm
σxx 7010
σyy 7010
σzz 7010
σxx 7075
σyy 7075
σzz 7075
σxx 7010 x-ray
σzz 7010 x-ray
σxx 7075 x-ray
σzz 7075 x-ray

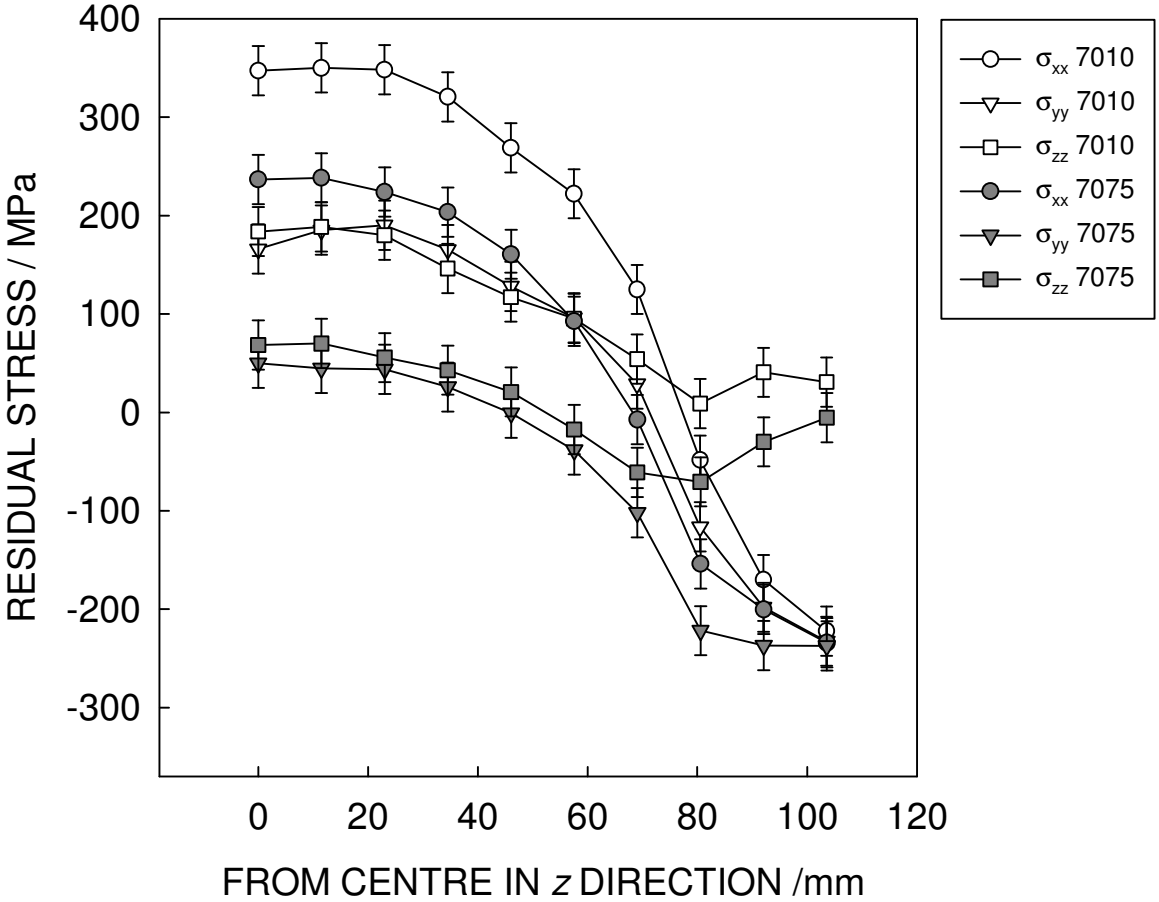
400
300
200
100
0
-100
-200
-300
RESIDUAL STRESS / MPa
0
20
40
60
80
100
120
FROM CENTRE IN z DIRECTION /mm
σxx 7010
σyy 7010
σzz 7010
σxx 7075
σyy 7075
σzz 7075

Figure 6 Residual stresses in the cold water quenched forgings measured from the central vertex out towards the three surfaces (as shown in Figure 2). In the top figure, the 7075 x-ray surface stresses are displaced to larger *x* for clarity. In the top figure the σ_{xx} component should approach zero as the surface is approached, in the middle figure, σ_{yy} and the bottom, σ_{zz}

A deep hole drilled residual stress measurement was made on the 7075 forging 12 months after solution heat treatment. The intervening period allowed natural aging to occur, strengthening the material. However, it was still expected that yielding would be encountered during the measurement so the incremental technique was used (7075 and 7010 uniaxial tensile test samples cold water quenched at a rate of approximately 300°C .s^{-1} and then tested immediately have a 0.1% proof stress of 140-150 MPa). The results of the iDHD measurement are shown in Figure 7. The iDHD residual stresses were significantly different to the neutron diffraction measurements especially for the σ_{yy} component in the interior of the forging. The iDHD values did show the same trends as the neutron diffraction measurements, and the compressive stresses determined towards the surface were in closer agreement with the neutron diffraction measurements. A conventional DHD analysis of hole diameter measurements made on the extracted core after completion of the iDHD measurement confirmed the presence of plasticity at approximately -65 < *z* < 65 mm which corresponds to the triaxially stressed centre of the forging.

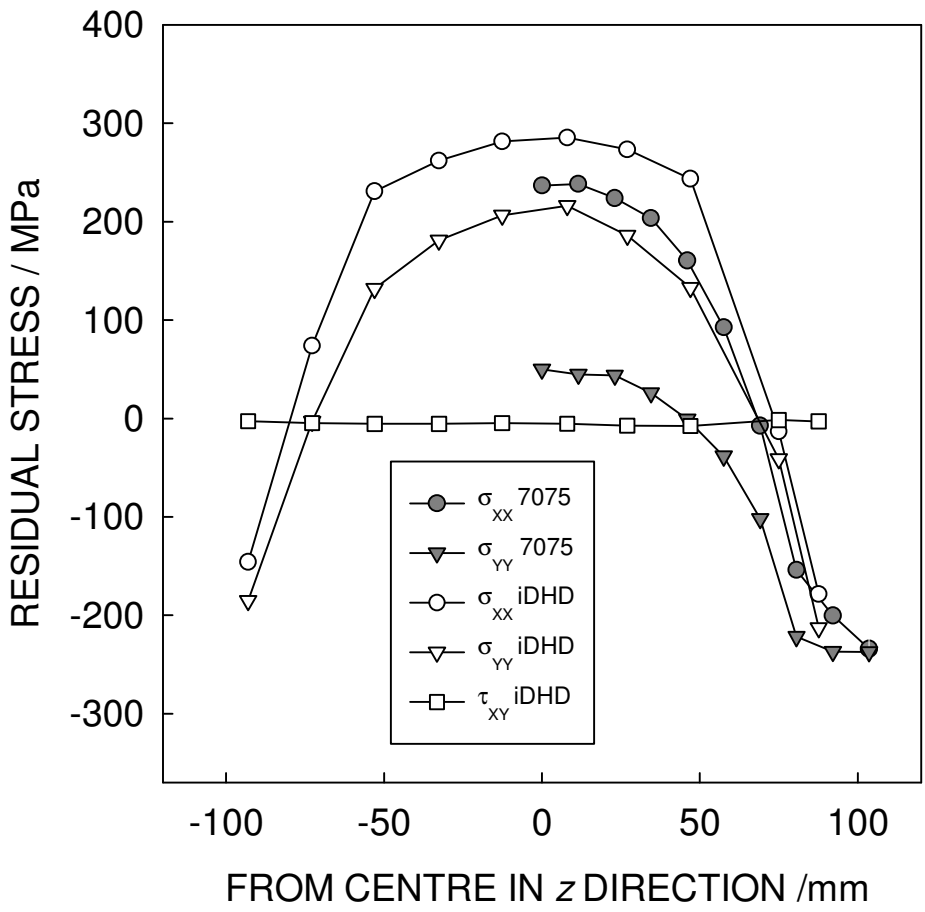

Figure 7 Incremental DHD σ_{xx} σ_{yy}, and τ_{xy} residual stresses made on the 7075 forging compared to σ_{xx} and σ_{yy} determined by neutron diffraction.

A deep hole drilled residual stress measurement was also made on the 7010 forging 16 months after solution heat treatment. This again had allowed natural aging to occur, strengthening the material, (the uniaxial 0.1% proof stress of 7010 after 16 months natural aging is approximately 350 MPa). The results of the iDHD

measurement are shown in Figure 8. In this case there was good correlation of the σ_{xx} residual stresses but the iDHD technique still appeared to overestimate the σ_{yy} residual stresses when compared to the neutron diffraction results. The iDHD values did show the same trends as the neutron diffraction measurements. A qualitative assessment of the degree of plasticity occurring during the deep hole measurement on the 7010 forging did suggest that this was less than that in the 7075 forging.

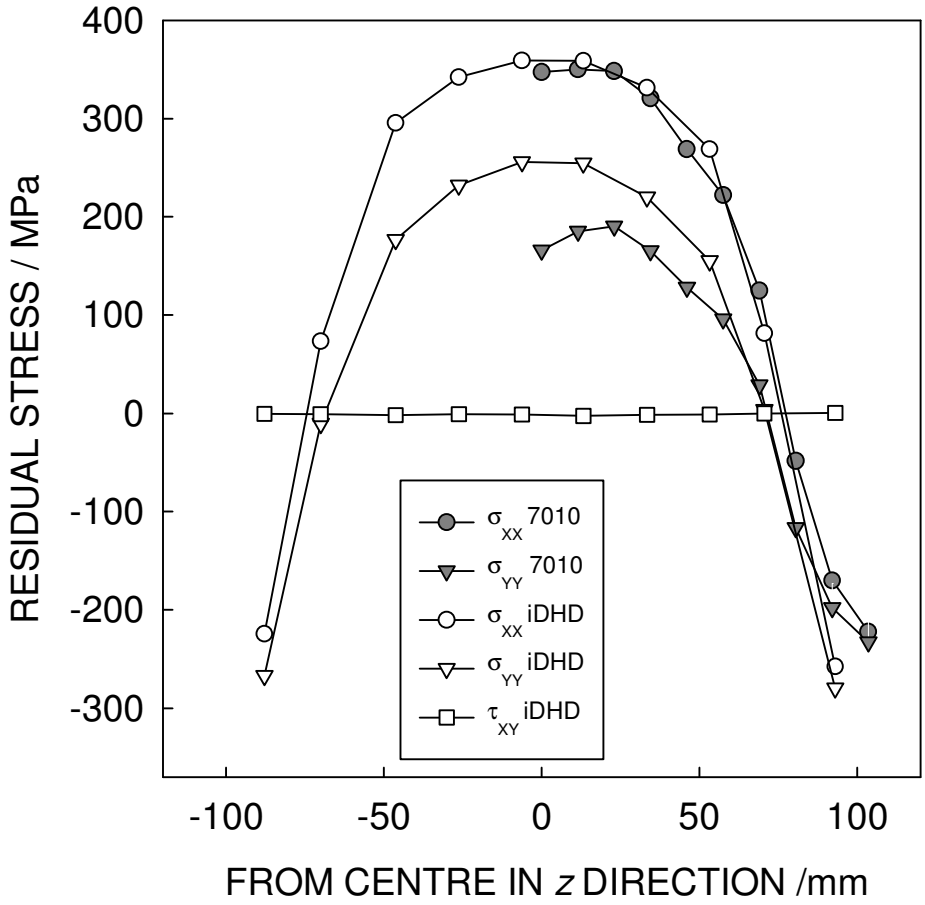

Figure 8 Incremental DHD σ_{xx} σ_{yy}, and τ_{xy} residual stresses made on the 7010 forging compared to σ_{xx} and σ_{yy} determined by neutron diffraction.

3.2 Though thickness hardness and microstructural variation

The influence of the different quench sensitivities of these two alloys can be clearly seen in Figure 9. In this figure the Vickers indentation hardness along the length of the extracted iDHD cores is reported, after over aging (T7x), along with a quench factor analysis prediction of hardness.[28]. 7010 is inherently harder than 7075 but displays only a minor variation along its length confirming the relative lack of quench sensitivity. In contrast, 7075 is significantly softer in the interior compared to the surface. The hardness of the cores had also been assessed prior to artificial aging i.e. in the naturally aged (W) condition. Both cores naturally aged to give very similar hardness distributions to those subsequently produced by overaging. In the case of the 7075 core, the hardness magnitudes were actually larger in the naturally aged (W) core. The lowering of the hardness in the over aged condition observed in the 7075 core when compared to the W condition is caused by precipitate reversion. Examination in the optical microscope did not reveal a microstructural reason for the hardness inversion observed at the ends of the cores. This was determined to be caused by the reduced constraint in the resin mounted cores allowing for a larger indentation. The overaging heat treatments were 10 hours at 120°C followed by 8 hours at 172°C for 7010, and 7 hours at 105°C plus 9 hours at 175°C for 7075. Both cores were artificially aged after having received the same period of natural aging.

To qualitatively assess the affect of quench sensitivity, samples for examination in the transmission electron microscope were prepared from the iDHD cores. Samples corresponding to the surface and centre of the forgings were electropolished to electron transparency and examined. Figure 10 displays typical microstructures from 7075 samples. The top pair of pictures are typical of the microstructure at the edge of the extracted DHD core (forging surface) and the bottom pair are from material at the centre of the extracted core (centre of the forging). The microstructure consisted of well defined sub-grains, an absence of dislocation substructures within sub-grains, coarse dispersoids (not shown in the pictures) and a very large number of relatively large Mg, Zn rich precipitates as shown in all the pictures. There was a minor variation in precipitate size from surface to centre. In contrast, the 7010 microstructure, as shown in Figure 11 was characterised by fine well recovered sub-grains, fine Al_3Zr spherical dispersoids and an almost complete absence of detectable Mg, Zn rich precipitates in both the surface and centre of the forging. In some areas of the TEM foils it was possible to find evidence of precipitation but only from samples prepared from the forging centre. This precipitation was not as widespread or as coarse as that observed in 7075. This can be attributed to local chemical heterogeneity. The widespread precipitation of a Mg, Zn phase (almost certainly $MgZn_2$) observed in 7075 was the major microstructural difference between this alloy and 7010. Optical microscopy of the mounted iDHD cores confirmed the presence of coarse precipitation within grain interiors along almost the complete length of the 7075 core. However the 7010 core was characterised by decoration of sub-grain boundaries by coarse precipitates, the degree increasing towards the forging interior.

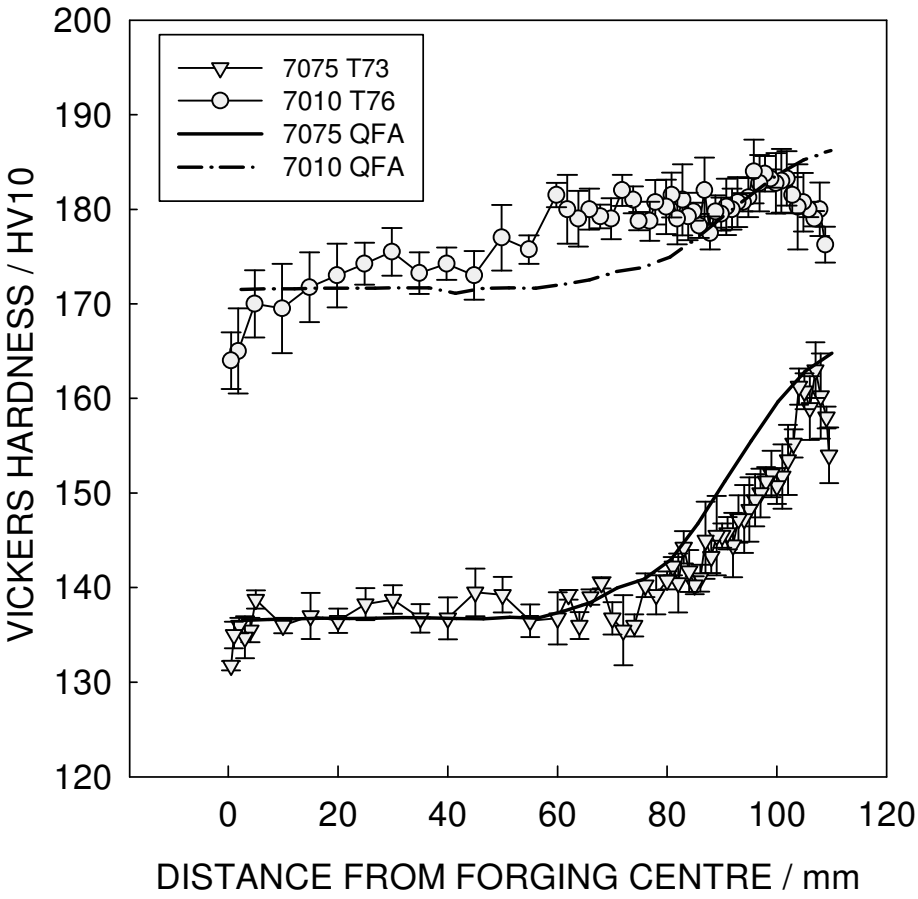

Figure 9 Indentation Vickers hardness measurement made along the core extracted during the iDHD procedure. T7x data relates to hardness measurements made after artificial over aging. Error bars correspond to ±1 standard deviation. Predicted hardness as determined by quench factor analysis (QFA) also inlcuded.

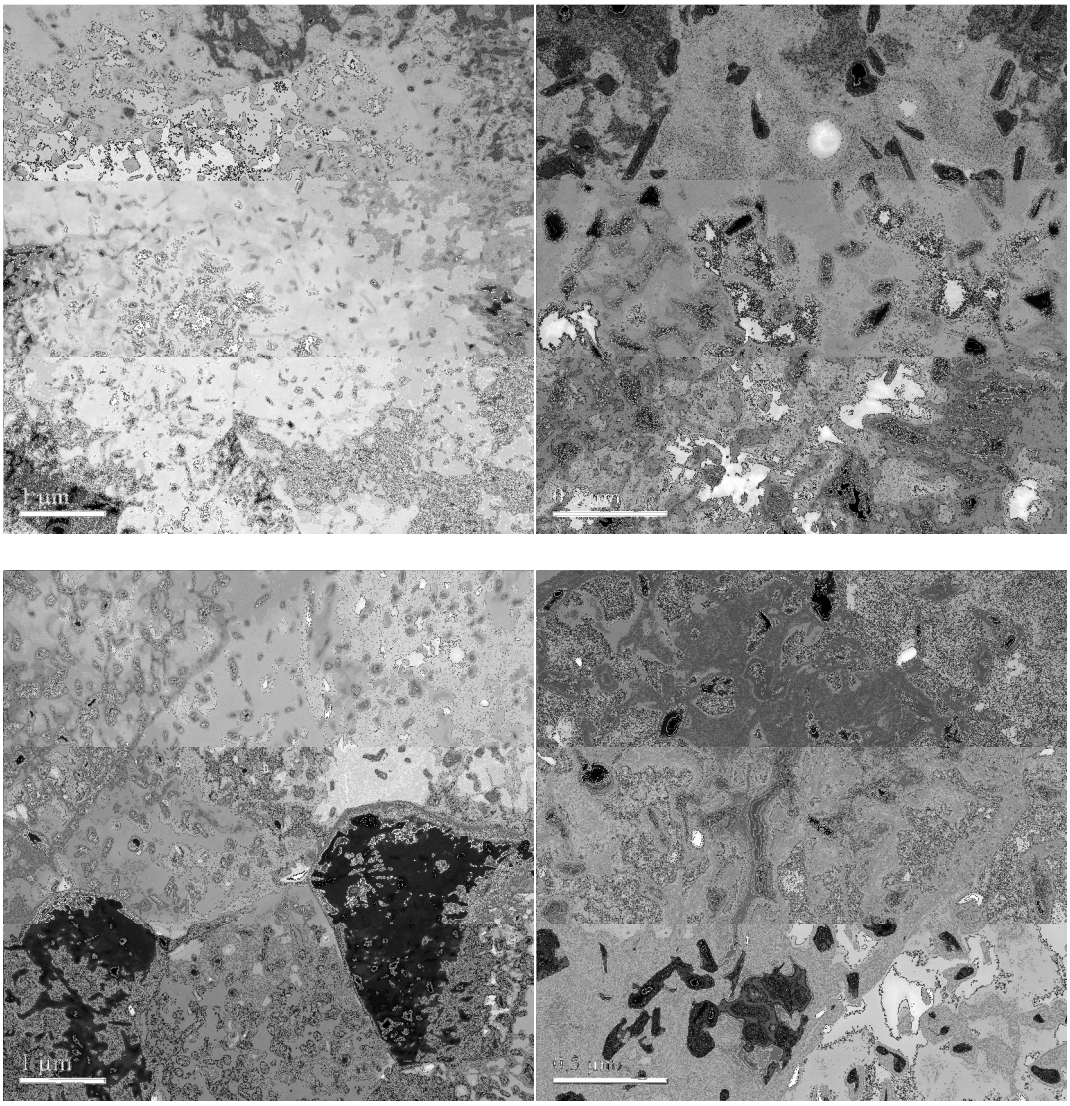

Figure 10 The top pair of figures correspond to typical TEM 7075 microstructure at the edge of the extracted DHD core (forging surface). Bottom pair are from material at the centre of the extracted core (centre of the forging).

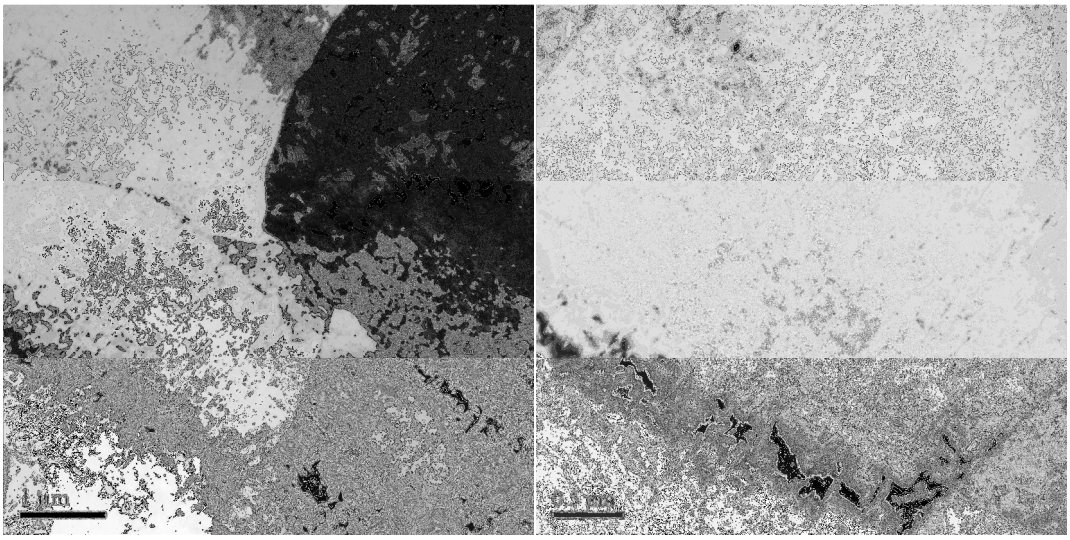

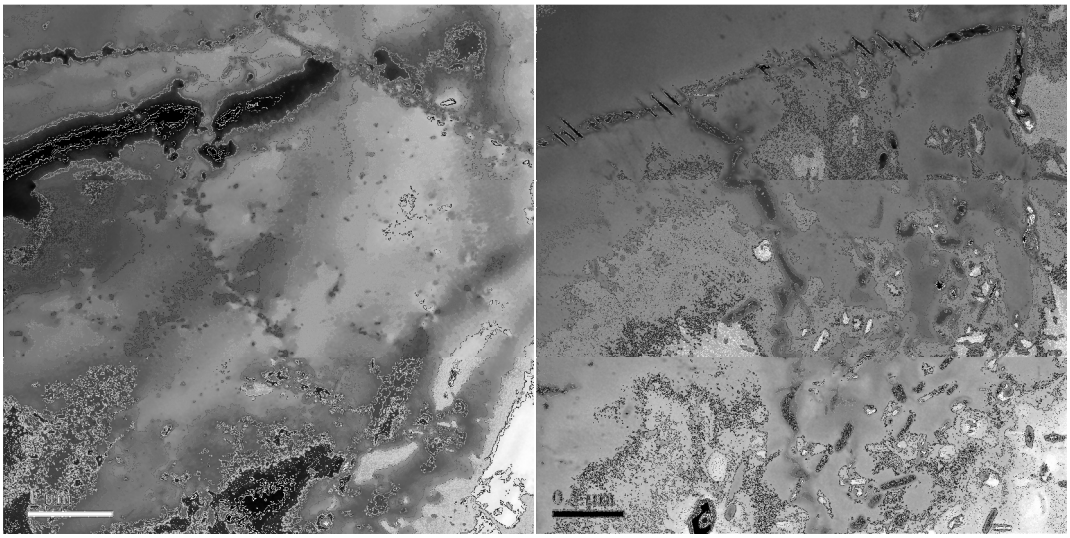

Figure 11 The top pair of figures correspond to typical TEM 7010 microstructure at the edge of the extracted DHD core (forging surface). The bottom pair are from material at the centre of the extracted core (centre of the forging).

3.3 Finite element analysis prediction of residual stress

The FEA model was run twice using upper and lower bound flow stress data to determine the range of residual stresses it would be reasonable to expect the 7075 and 7010 forgings to exhibit. This was done to highlight possible deficiencies present in the residual stress measurements. To evaluate the upper and lower bounds simply involved plotting calculated flow stresses using the Sheppard and Jackson data[25] against the temperature compensated strain rate *Z* (Zener-Holloman parameter) as shown in Figure 12. An upper and lower bound line was constructed empirically and the associated constitutive constants were used to generate the flow stress as a function of temperature and strain rate for the ABAQUS input file. The steady state flow stress was calculated using the following equation[29];

$$\sigma = \frac{1}{\alpha}\ln\left\{\left(\frac{Z}{A}\right)^{\frac{1}{n}} + \left[1+\left(\frac{Z}{A}\right)^{\frac{2}{n}}\right]^{1/2}\right\} \tag{4}$$

The temperature compensated strain rate, Z is given by

$$Z = \dot{\varepsilon}\exp\left(\frac{\Delta H}{RT}\right) \tag{5}$$

$\dot{\varepsilon}$ is the strain rate, *R* is the universal gas constant, *T* is the absolute temperature, ΔH is an activation energy related to that of self diffusion of aluminium, and *A*, α and *n* are alloy dependent constants.

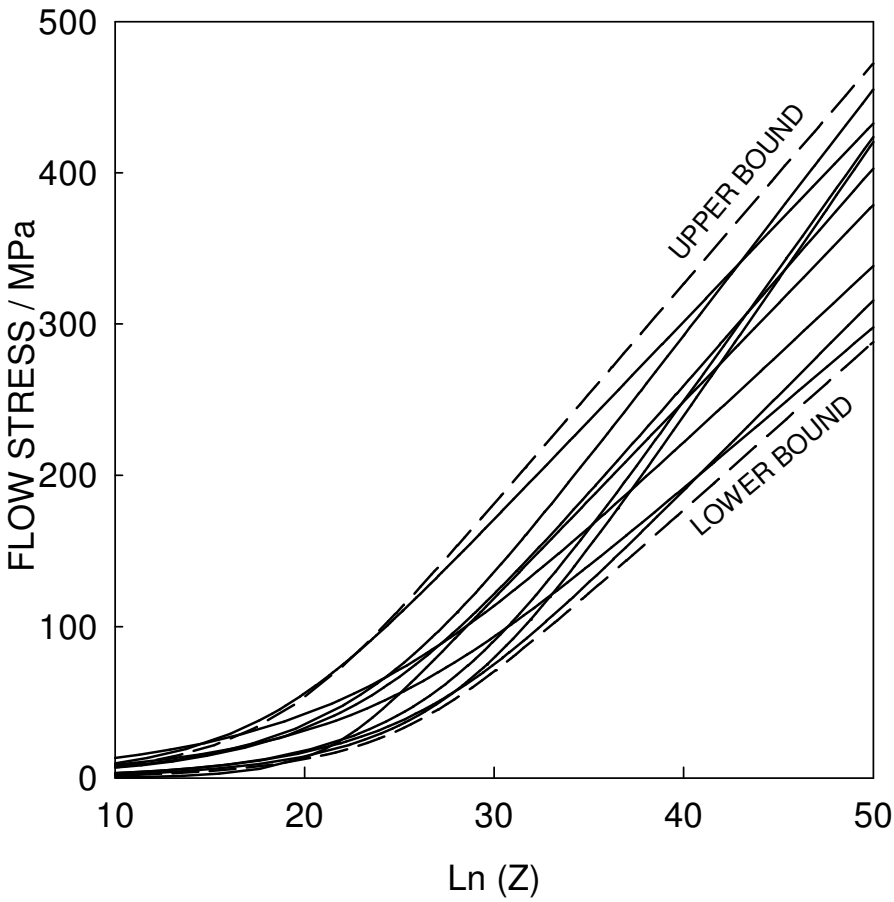

Figure 12 The flow stress of 7050, 7150 and 7075 as a function of the temperature compensated strain rate *Z*. The upper and lower bounds correspond to the flow stresses used in the FEA analysis. The lines between use the 7050, 7150 and 7075 flow stress data from Sheppard and Jackson[25]

The results of the FE analysis are shown in Figure 13. In this figure the upper and lower bound predictions of σ_{xx}, are reported along with σ_{yy} and σ_{zz} which for this orientation were identical. The other line scans displayed the same general characteristics. The upper bound FEA prediction was very close to the 7010 neutron diffraction observations for σ_{xx}, σ_{yy} and σ_{zz}. For 7075 only the lower bound σ_{xx} component gave a reasonable fit to the neutron diffraction data. The σ_{yy} and σ_{zz} neutron diffraction observations for 7075 were significantly lower than the lower bound FEA prediction in the forging interior. This does suggest an issue with the accuracy of the 7075 neutron diffraction measurements in the forging interior.

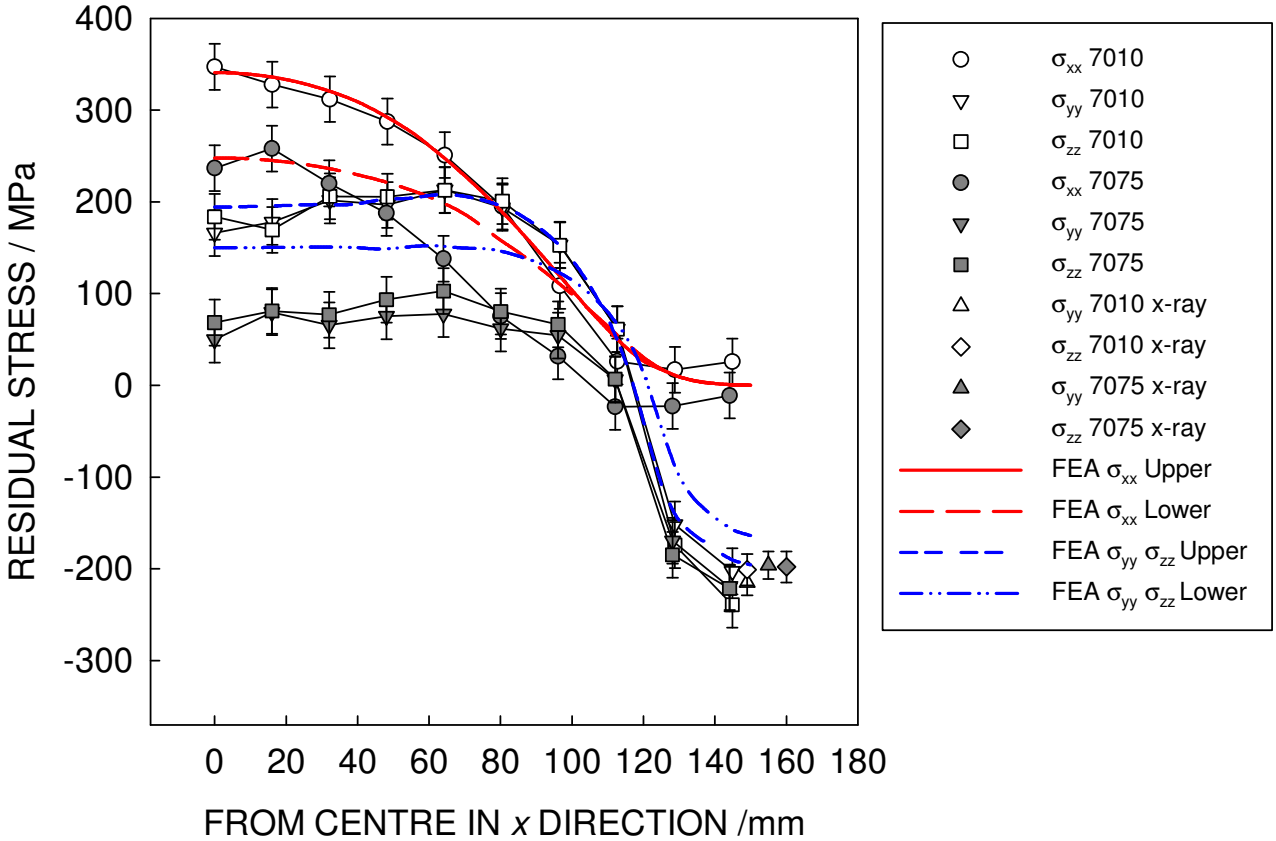

Figure 13 Upper and lower bound FEA predictions plotted with the neutron diffraction residual stresses replicated from the top plot of Figure 6. Measured from the central vertex out towards the surface defined by the *y* and *z* directions (as shown in Figure 2).

3.4 Lattice parameter measurements from the iDHD cores.

Measurements of the matrix lattice parameter on the extracted iDHD cores were made by neutron diffraction using the E3 instrument at HZB, Berlin. Measurements were made on the cores corresponding to the *x* and *y* directions of the forged blocks. It was assumed the cores would be approximately strain free due to the complete removal of the surrounding constraining material. The neutron diffraction 311 peak position (2θ) as a function of location along the cores (measuring d_{311}) is shown in Figure 14, with peak position converted to microstrain ($\varepsilon \times 10^{-6}$) by assuming the lattice parameter measured close to the surface exposed to the quench water corresponds to the d^{0}_{311} (~110 mm position in Figure 14). If significant microstructural variation existed along the cores due to the different cooling, (causing different degrees of solute supersaturation), this would be reflected in a shift in the peak position. There was scatter in these observations but there was a significant shift in the peak position of the 7075 core, but less so for the 7010 core. A small gauge volume was used for these measurements (1.5 mm^3) but it is possible certain observations were affected by the gauge volume exiting the sample or entering the recast layer in the trepanned core surface. The cause of a peak shift when the gauge volume is partly outside the sample is well documented.[30]

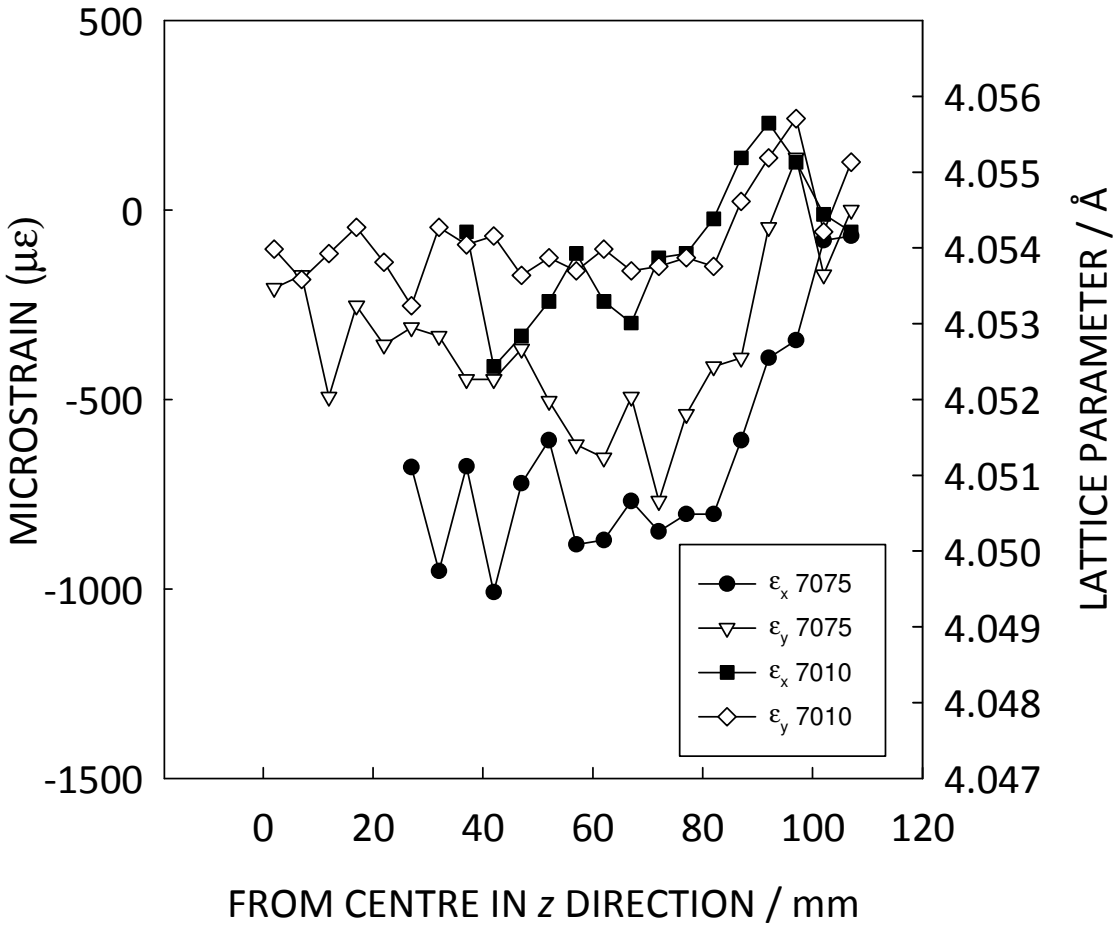

Figure 14 Variation in lattice parameter represented as microstrain along the extracted iDHD cores as determined by neutron diffraction sampling of the 311 interplanar spacing.

4 Discussion

Characterisation of the residual stresses in the 7010 and 7075 forgings is consistent with the usually reported pattern of surface compression balanced by subsurface tension. The magnitudes of the maximum and minimum residual stresses observed are similar to previous investigations conducted on other 7000 series aluminium alloys.[31-33] However, the residual stresses in the core of the 7075 forging when measured by neutron diffraction are much lower than those in the 7010 forging. Surface residual stresses in both forgings are similar at ~-200MPa and correlate well with surface x-ray measurements.

This investigation's primary task was to determine if quench sensitivity could influence residual stress magnitudes in heat treatable aluminium alloys. The neutron diffraction data certainly seems to suggest that in the centre of the forgings at least, the quench sensitive 7075 alloy will not support the high magnitude triaxial tensile residual stresses observed in the less quench sensitive alloy 7010. However, the similarity of the surface stresses and the fact that the FEA analysis suggests the residual stresses should be similar does call into question the accuracy of the neutron diffraction observations for the core of the 7075 forging, an issue that is addressed below. The iDHD measurements also confirm a difference between the two alloys with the interior 7010 residual stress magnitudes again being greater than the 7075. The iDHD 7010 observations were in reasonable agreement with the neutron diffraction observations but the iDHD measurements for the 7075 forging were significantly larger than the neutron diffraction residual stresses, especially in the *y* direction within the forging. The 7075 iDHD measurement was made 12 months after solution treatment and 4 months before the 7010 measurement. By treating the deep hole measurement as a conventional DHD experiment, and measuring the core diameters after sectioning of the core from the forging, it was clear that significant

plasticity had occurred during the trepanning operation. In contrast, the 7010 sample did not exhibit plastic deformation to the same extent. There are two reasons for this, the first is that the 7010 had an extra 4 months of natural aging resulting in a stronger material, and secondly 7010 is less quench sensitive than 7075, so would be expected to exhibit a greater natural aging response anyway. It is quite clear from the hardness data in Figure 9 that 7010 is significantly stronger than 7075. Unlike the conventional DHD process, the iDHD extension accounts for any plasticity that arises during the measurement due to high magnitude residual stresses. However, the corrections due to plasticity are essentially empirical in nature, differing from the conventional DHD technique which is formulated in terms of an exact elasticity solution. In the measurements undertaken in this paper, where there are high magnitude residual stresses over a large measurement volume, it is not possible to state with any certainty if these observations are significant.

Microstructural examination of the extracted iDHD cores clearly indicates the difference between the quench sensitivity of the two alloys. 7075 has a chromium addition and this promotes the formation of incoherent solute rich dispersoids. 7010 is a more modern composition and substitutes the chromium for a zirconium addition which results in solute free coherent Al_3Zr dispersoids.[34] The indentation hardness measurements on the iDHD cores in Figure 9 also illustrates the quench sensitivity differences as do the E3 lattice parameter observations in Figure 14.

If the lattice parameter of pure Al is assumed to be 4.0496Å then the influence of the alloying elements in solid solution can be calculated using literature data.[35] For both 7010 and 7075 (using the specification nominal compositions), the lattice parameter is 4.056Å. This assumes that all the Zn, Mg and Cu atoms are in solid solution. The element that has the biggest influence on lattice parameter is Mg and this causes an increase, whereas Zn and Cu cause a small decrease. As the surface of the forgings is approached the lattice parameter does tend towards the value expected with all the solute in solid solution, as shown in Figure 14. The smaller lattice parameter associated with the interior of the forgings will tend to increase the magnitude of the tensile residual stresses calculated from the neutron diffraction observations. This can go some way to explaining the discrepancy between the 7010 and 7075 neutron diffraction observations. Using a corrected mean interior lattice parameter of 4.052Å increases the interior residual stresses in the 7075 forging to the same magnitude as those observed in the 7010 forging and improves the correlation with the iDHD measurements.

In summary, for this experiment it is clear the quench sensitivity of the 7075 alloy renders impractical the use of a single d^0 sample taken from the rapidly cooled corner of the forging. For the less quench sensitive 7010 alloy, a single d^0 sample will suffice. However the influence of quench sensitivity means that for accurate neutron diffraction residual stresses, a through thickness d^0 sample like the iDHD core is required. When this is utilised then the residual stresses in the two forgings are similar. However the iDHD measurement itself does indicate a difference between the two alloys with the 7010 forging reporting larger magnitude stresses. Due to the plasticity encountered and the limitations of the technique it is not possible to state with any certainty if these observations are significant. With regard to the initial objective of this investigation then it is not possible to clearly state if the more quench sensitive alloy will result in measurably lower residual stresses. Surface stresses measured using both neutron diffraction and x-ray diffraction indicated similar magnitude compressive stresses for the two forgings which would lead one to expect to find similar residual stress in the interior. Further investigations using quench factor analysis might permit the prediction of lattice parameter. As illustrated in Figure 9, using QFA can predict the variation in hardness quite accurately. While it could not implemented here because the forgings were naturally aged only, there is no reason why this empirical technique cannot be extended to the prediction of lattice parameter for use in neutron diffraction experiments.

5 Conclusions

Measurement of the residual stresses present in cold water quenched 7010 and 7075 large rectilinear forgings by neutron diffraction follows the expected pattern of biaxial compression in the surface balanced by triaxial tensile stresses in the forging interiors.

Compressive surface residual stresses when measured by neutron diffraction and x-ray diffraction are in close agreement for both forgings.

The neutron diffraction observations for the interior of the forgings show clear differences in the tensile residual stress magnitudes developed. The less quench sensitive 7010 forging exhibits much higher tensile residual stresses compared to the 7075 forging.

The difference in the neutron diffraction residual stress observations between the two alloys is attributed to the use of single d^0 samples sectioned from a rapidly cooled corner of each block. If a through thickness d^0 sample is used for the 7075 forging then the interior residual stresses of both forgings are very similar.

Through thickness microstructural variations arising from loss of solute in the form of coarse second phase precipitation cause large changes in the lattice parameter of the quench sensitive 7075. In the 7010 forging precipitation does occur on grain and sub-grain boundaries but the change in lattice parameter is small in comparison.

The incremental deep hole drilling measurements show the same trends as the neutron diffraction results but the magnitudes are significantly different, with the iDHD residual stresses being larger than the neutron diffraction data

The incremental deep hole drilling measurements also suggest the 7010 forging is capable of supporting higher tensile residual stress in the forging interior.

The difference in residual stresses between the two forgings arising from the iDHD measurements is potentially due to the greater plasticity encountered in the 7075 forging.

The tensile core residual stress magnitudes in both 7075 and 7010 forgings greatly exceed the uniaxial as quenched yield strength.

The neutron diffraction and iDHD measurement made here were not able to isolate the affects of quench sensitivity on residual stress magnitudes. Limitations in the d^0 utilised and plasticity effects during the iDHD did not permit the quantification of the influence of precipitation occurring during quenching and the concomitant lowering of the flow stress.

Acknowledgements

This investigation has been supported by the European Commission under the 6th Framework Programme project known as COMPACT (AST4-CT-2005-516078), which contributes to the thematic priority “Strengthening Competitiveness” of the European aircraft industry. Experiments at the ISIS Pulsed Neutron and Muon Source were supported by beam time allocations from the Science and Technology Facilities Council. The authors acknowledge the beam time and facilities provided by the Helmholtz centre, Germany. The authors would also like to thank John Lammas of Mettis Aerospace, UK for supplying the material and arranging the forging and heat treatment.

List of Tables

Alloy	wt%Zn	wt%Mg	wt%Cu	wt%Zr	wt%Fe	wt%Si	wt%Ti	wt%Mn	wt%Cr
7010	6.7-5.7	2.6-2.1	2.0-1.5	0.16-0.10	0.15max	0.12max	0.06max	0.10max	0.05max
7075	6.1-5.1	2.9-2.1	2.0-1.2	0.05max	0.5max	0.4max	0.2max	0.3max	0.3-0.2

References

[1] R.E. Kleint, F.G. Janney, Stress Relief in Aluminum Forgings, Light Metal Age, 2 (1958) 14-21.

[2] R. Becker, M.E. Karabin, J.C. Liu, R.E. Smelser, Distortion and residual stress in quenched aluminum bars, Journal of Applied Mechanics-Transactions of the Asme, 63 (1996) 699-705.

[3] D.A. Tanner, J.S. Robinson, R.L. Cudd, Relief of residual stresses in aluminium alloy 7010, in: Proceedings of the The Sixth International Conference on Residual Stresses ICRS-6, 10-12 July 2000, Institute of Materials, Oxford, UK, 2000, pp. 1299-1306.

[4] J.T. Staley, Quench factor analysis of aluminium alloys, Mater. Sci. Technol., 3 (1987) 923-935.

[5] R.J. Flynn, J.S. Robinson, The application of advances in quench factor analysis property prediction to the heat treatment of 7010 aluminium alloy, in: D. A.G.Olabi, P.S.J. Hashmi (Eds.) Proceedings of the International Conference on Advances in Materials and Processing Technologies, AMPT2003, Dublin City University, Dublin, Ireland, 2003, pp. 123-126.

[6] D. Godard, P. Archambault, S. Denis, E. Gautier, F. Heymes, Modelling of heat treatment residual stresses. Application to high strength aluminium alloys including precipitation effects, in: Proceedings of the 7th International Seminar of IFHT: Heat treatment and surface engineering of light alloys, Budapest, Hungary, 1999, pp. 249-257.

[7] IS0/TTA3, Polycrystalline materials – Determination of residual stresses by neutron diffraction, in: Technology trends assessment, International standardisation organisation, 2001.

[8] D.C.I.T. 21432, Non-destructive testing. Standard test method for determining of residual stresses by neutron diffraction, in, British Standards Institute, 2005.

[9] G.S. Pawley, Unit-cell refinement from powder diffraction scans, J. Appl. Crystallogr., 14 (1981) 357-361.

[10] M.T. Hutchings, P.J. Withers, T.M. Holden, T. Lorentzen, Introduction to the characterisation of residual stress by neutron diffraction, CRC Press, Boca Raton, FL, USA, 2005.

[11] M.E. Fitzpatrick, A.T. Fry, P. Holdway, F.A. Kandil, J. Shackleton, L. Suominen, Determination of residual stresses by X-ray diffraction, in, NPL, 2002.

[12] I.C. Noyan, J.B. Cohen, Residual Stress [Measurement by Diffraction and Interpretation], in: Residual Stress [Measurement by Diffraction and Interpretation], Springer-Verlag, New York, 1987.

[13] V.M. Hauk, E. Macherauch, A useful guide for X-ray stress evaluation (XSE), Advances in X-ray Analysis, 27 (1983) 81-89.

[14] B.D. Cullity, S.R. Stock, Elements of x-ray diffraction, 3d ed., Prentice Hall., Upper Saddle River, New Jersey, USA, 2001.

[15] E.J. Kingston, D. Stefanescu, A.H. Mahmoudi, C.E. Truman, D.J. Smith, Novel Applications of the Deep-Hole Drilling Technique for Measuring Through-Thickness Residual Stress Distributions Journal of ASTM International 3(2006) 12.

[16] D.M. Goudar, S. Hossain, C.E. Truman, E.J. Kingston, D.J. Smith, Uncertainties in Triaxial Residual Stress Measurements, Materials Science Forum, 681 (2011) 498-503.

[17] A.H. Mahmoudi, S. Hossain, C.E. Truman, D.J. Smith, M.J. Pavier, A New Procedure to Measure near Yield Residual Stresses Using the Deep Hole Drilling Technique, Exp. Mech., 49 (2009) 595-604.

[18] Hibbitt, Karlsson, Sorensen, ABAQUS Finite element code, in, Pantuck, RI, 2007.

[19] Y.S. Touloukian, H. Buyco, Specific heat: Metallic elements and alloys, in: Thermophysical properties of matter, IFI/Plenum Press, New York, 1970.

[20] Y.S. Touloukian, R.W. Powell, C.Y. Ho, P.G. Klemens, Thermal Conductivity: Metallic elements and alloys, in: Thermophysical properties of matter, IFI/Plenum Press, New York, 1970.

[21] P. Jeanmart, J. Bouvaist, Finite element calculation and measurement of thermal stresses in quenched plates of high-strength 7075 aluminium alloy, Mater. Sci. Technol., 1 (1985) 765-769.

[22] D.M. Trujillo, INTEMP, in, TRUCOMP, FOUNTAIN VALLEY, CA., 92708, USA, 2003, pp. Inverse Heat Transfer Analysis.

[23] Y.S. Touloukian, R.K. Kirby, R.E. Taylor, P.D. Desai, Thermal expansion: Metallic elements and alloys, in: Thermophysical properties of matter, IFI/Plenum Press, New York, 1970.

[24] M. Handbook, Heat Treating, in: Metals Handbook, ASM International, 1981, pp. 696-697.

[25] T. Sheppard, A. Jackson, Constitutive equations for use in prediction of flow stress during extrusion of aluminium alloys, Mater. Sci. Technol., 13 (1997) 203-209.

[26] S.R. Yazdi, D. Retraint, J. Lu, Study of through-thickness residual stress by numerical and experimental techniques, J. Strain Anal. Eng. Des., 33 (1998) 449-458.

[27] D.M. Walker, R.Y. Hom, Residual stress analysis of aircraft aluminum forgings, Adv. Mater. Process., 160 (2002) 57-60.

[28] J.T. Staley, M. Tiryakioglu, The use of TTP curves and quench factor analysis for property prediction in aluminum alloys, in: Proceedings from Materials Solutions Conference 2001, Nov 5-8 2001, ASM International, Indianapolis, IN, United States, 2001, pp. 6-15.

[29] C.M. Sellars, W.J.M. Tegart, Hot Workability, International Metallurgical Reviews, 17 (1972) 1-24.

[30] P.J. Webster, G. Mills, X.D. Wang, W.P. Kang, T.M. Holden, Impediments to efficient through-surface strain scanning, Journal of Neutron Research, 3 (1996) 223 - 240.

[31] J.S. Robinson, S. Hossain, C.E. Truman, E.C. Oliver, D.J. Hughes, M.E. Fox, Influence of cold compression on the residual stresses in 7449 forgings, Advances in X-ray Analysis, 52 (2009) 667-674.

[32] M.B. Prime, M.R. Hill, Residual stress, stress relief, and inhomogeneity in aluminum plate, Scr. Mater., 46 (2002) 77-82.

[33] M.B. Prime, M.A. Newborn, J.A. Balog, Quenching and cold-work residual stresses in aluminium hand forgings: contour method measurement and FEM prediction, in: THERMEC'2003: Processing & Manufacturing of Advanced Materials, Madrid, Spain, 2003.

[34] S.D. Liu, Q.M. Zhong, Y. Zhang, W.J. Liu, X.M. Zhang, Y.L. Deng, Investigation of quench sensitivity of high strength Al-Zn-Mg-Cu alloys by time-temperature-properties diagrams, Materials & Design, 31 (2010) 3116-3120.

[35] J.E. Hatch, Constitution of alloys, in: Aluminum: Properties and Physical Metallurgy, ASM, 1984, pp. 48-50.